Global Optimization of 8–10 Atom Palladium–Iridium Nanoalloys at the DFT Level

ARTICLE *in* THE JOURNAL OF PHYSICAL CHEMISTRY A · DECEMBER 2013

Impact Factor: 2.69 · DOI: 10.1021/jp408519z · Source: PubMed

3 AUTHORS:

Jack Davis
University of Birmingham
6 PUBLICATIONS **16** CITATIONS
SEE PROFILE

Sarah L Horswell
University of Birmingham
38 PUBLICATIONS **570** CITATIONS
SEE PROFILE

Roy L Johnston
University of Birmingham
240 PUBLICATIONS **6,545** CITATIONS
SEE PROFILE

THE JOURNAL OF PHYSICAL CHEMISTRY A

Article

pubs.acs.org/JPCA

Global Optimization of 8−10 Atom Palladium−Iridium Nanoalloys at the DFT Level

Jack B. A. Davis, Sarah L. Horswell, and Roy L. Johnston*

School of Chemistry, University of Birmingham, Edgbaston, B15 2TT, Birmingham, United Kingdom

Supporting Information

ABSTRACT: The global optimization of $Pd_nIr_{(N-n)}$ N = 8−10 clusters has been performed using the Birmingham Cluster Genetic Algorithm (BCGA). Structures were evaluated directly using density functional theory (DFT), which has allowed the identification of Ir and Ir-rich PdIr cubic global minima, displaying a strong tendency to segregate. The ability of the searches to find the putative global minimum has been assessed using a homotop search method, which shows a high degree of success. The role of spin in the system has been considered through a series of spin-restricted reoptimizations of BCGA-DFT minima. The preferred spin of the clusters is found to vary widely with composition, showing no overall trend in lowest-energy multiplicities.

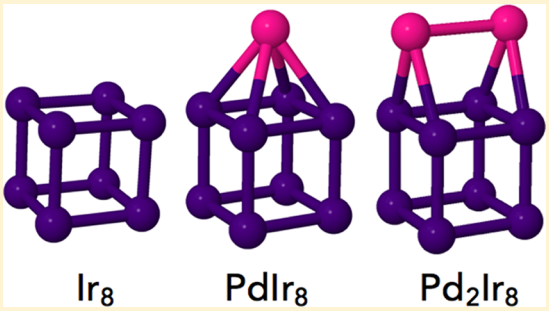

INTRODUCTION

It is well-established that alloying can increase the activity and/or the selectivity of metal catalysts.[1] On the nanoscale, nanoalloys have the potential to combine this alloying effect with tunable properties for use in specific processes.[2,3] The structural characterization of nanoalloys is a vital step toward understanding their role in catalysis. Several methods exist, including basin-hopping and genetic algorithms.[2,4,5]

Noble metals are being widely investigated for use in catalysis. Small iridium clusters show promise in several processes, including activity in the ring-opening catalysis of naphthenes.[6] Palladium−iridium nanoalloy catalysts show activity in tetralin hydroconversion,[7,8] the hydrogenation of benzonitrile,[9] and the preferential oxidation of CO for the elimination of impurities in H_2 production.[10]

Previous density functional theory (DFT) studies of small Ir clusters, using ultrasoft pseudopotentials and PBE exchange−correlation functionals, have predicted a simple cubic arrangement for Ir clusters up to 48 atoms.[11,12] This is coupled with results from CCSD calculations, which also predict a cubic structure.[13] DFT studies of small Pd clusters, using the SVP basis set and BP-86 exchange−correlation functional, have also been conducted.[14] These, however, were not exhaustive searches of conformational space.

In this study, the global optimization of $Pd_nIr_{(N-n)}$ N = 8−10 clusters is performed, where N is the total number of atoms and n the number of Pd atoms. Global optimization is carried out using the Birmingham Cluster Genetic Algorithm (BCGA), which allows global optimization directly at the DFT level, utilizing an interface to the plane wave DFT PWscf code within Quantum Espresso (QE).[15] This provides an unbiased search starting from entirely random coordinates and enables the identification of size-specific effects not usually described by empirical methods, such as the Gupta potential.[16,17]

As a result of the $5d^76s^2$ ground-state electronic configuration of Ir and low-lying states originating from its $5d^86s^1$ configuration, the spin of any Ir_N and $Pd_nIr_{(N-n)}$ clusters must be considered.[18] 'The influence of spin has not been widely investigated for Ir clusters but has been shown to play a role.[13] The spin of the pure and alloyed clusters is investigated through the use of spin-restricted calculations on BCGA-DFT global minima using atomic-orbital-based DFT calculations in the NWChem package.[19] Spin-unrestricted QE calculations are not carried out within the BCGA due to the high computational cost of converging both the spin and geometry of the system.

METHODOLOGY

In the present study, the BCGA, using an interface to the PWscf DFT code within QE, is used for the global optimization of Pd−Ir nanoalloy structures. The BCGA is a genetic algorithm for the structural characterization of nanoparticles and nanoalloys.[5] The interface to QE allows the energy landscape of a system to be explored at the DFT level.[17]

The initial population consists of a number of randomly generated cluster geometries, N_{pop} = 10−40. The BCGA is a "Lamarckian" type GA, with fitness being assigned to locally minimized structures at each step of the GA according to their energy. Structures with the lowest energies have the highest fitness. Here, the energy of each member of the population will be calculated using a PWscf DFT calculation.

Parent clusters are selected for crossover through roulette wheel selection.[5] Crossover occurs according to the Deaven and Ho cut and splice method and continues until a

Received: August 26, 2013
Revised: November 27, 2013
Published: December 13, 2013

   dx.doi.org/10.1021/jp408519z | J. Phys. Chem. A 2014, 118, 208−214

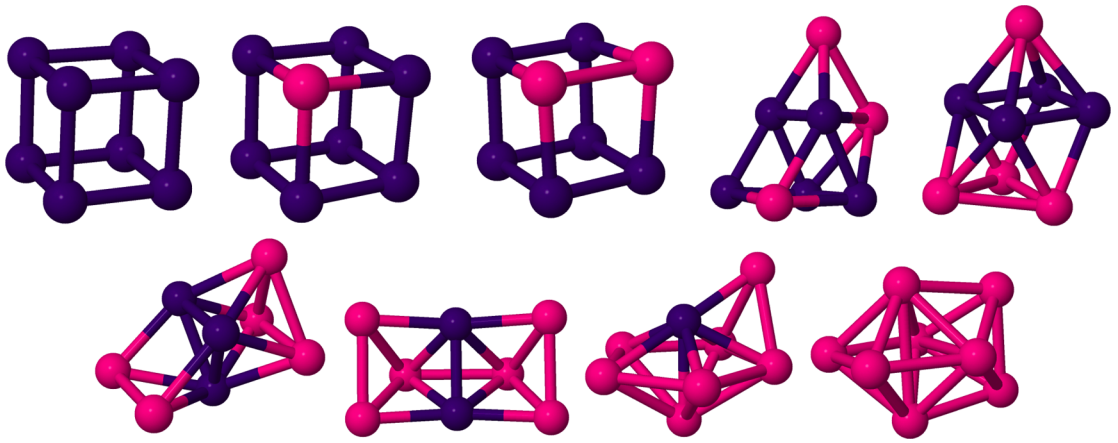

Figure 1. Global minima for eight-atom $Pd_nIr_{(8-n)}$ clusters. Pd and Ir are shown in pink and purple, respectively.

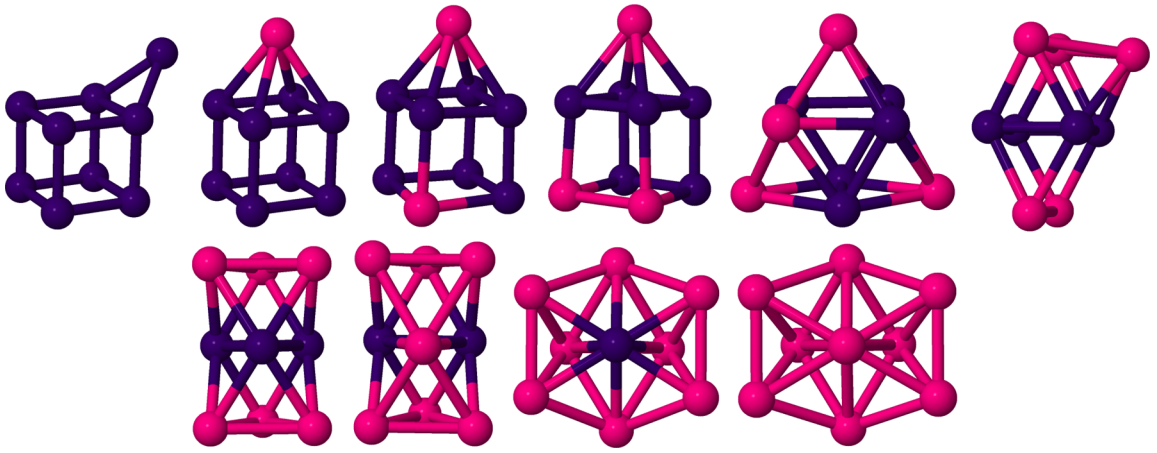

Figure 2. Global minima for nine-atom $Pd_nIr_{(9-n)}$ clusters.

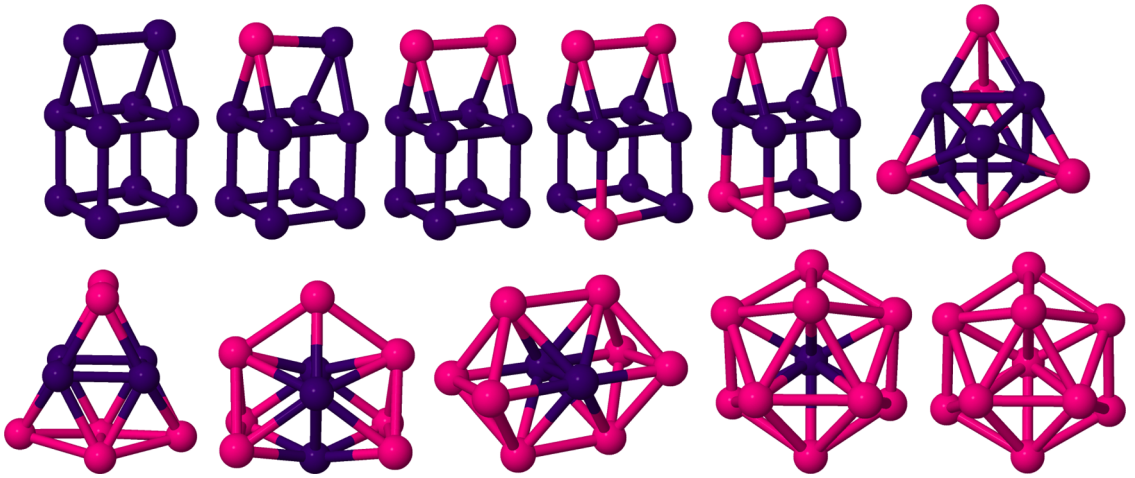

Figure 3. Global minima for 10-atom $Pd_nIr_{(10-n)}$ clusters.

predetermined number of offspring, N_{off}, have been generated.[20] Mutation is carried out to ensure that population diversity is maintained. All members of the population have a probability, p_{mut}, of being selected for mutation. The BCGA contains a number of mutation schemes, including, atom displacement, twisting, cluster replacement, and atom permutation.

This process of selection, crossover, and mutation is repeated for a number of generations. The population is considered converged when the range of energies remains unchanged for a number of generations.[5]

QE calculations were carried out using PAW pseudopotentials, taking scalar relativistic effects into account.[21] The Perdew–Burke–Ernzerhof (PBE) exchange–correlation functional is used within the generalized gradient approximation (GGA).[22,23] An energy cutoff (E_{cut}) of 55 Ry is used with the default density cutoff to ensure fast SCF steps and quick convergence. The Fermi–Dirac smearing scheme, with a

dx.doi.org/10.1021/jp408519z | J. Phys. Chem. A 2014, 118, 208–214

smearing width of 0.02, was used to improve metallic convergence.

Spin-polarized reminimizations of the BCGA-DFT global minima were carried out with the orbital-based DFT package NWChem, using Def2-TZVP basis sets and PBE exchange–correlation functionals.[19,24]

Excess energies (Δ) were calculated to determine the stability of bimetallic clusters relative to the monometallic species or the energy associated with alloying. Δ is defined as

$$\Delta = E(A_mB_n) - m\frac{E(A_N)}{N} - n\frac{E(B_N)}{N} \quad (1)$$

DFT binding energies (E_b) are computed from

$$E_b = \frac{1}{N}[E_{(A_mB_n)} - mE_A - nE_B] \quad (2)$$

where $E_{A_mB_n}$ is the total energy of the cluster and $E_{A/B}$ are the energies of the single atoms.

RESULTS AND DISCUSSION

The putative global minima for $Pd_nIr_{(N-n)}$ N = 8–10 clusters are shown in Figures 1–3. Tables listing the structures and point groups of all clusters are given in the Supporting Information.

The Ir_8 global minimum (GM) is a cube, as previously reported.[11−13] When doped with up to two Pd atoms, the cube remains the GM. When three Pd atoms are added, the structure changes to a C_s structure based on a capped trigonal prism with a four-atom square Ir fragment. The Pd_8 GM is a D_{2d} dodecahedral structure, as previously reported.[14] Upon successive iridium doping, the structure changes to a C_s capped pentagonal bipyramid and then to a C_{2h} structure formed from two edge-sharing square pyramids.

The Ir_9 GM is an edge-bridged cube, also as previously reported.[12] As Pd is doped into the structure, the cap switches from an edge to a face with Pd occupying the capping site. This is the case for $PdIr_8$, Pd_2Ir_7, and Pd_3Ir_6. The first Pd dopant caps a face, with the second and third forming a Pd–Pd bond on the face opposite the cap. Pd_4Ir_5 and Pd_5Ir_4 both retain square Ir fragments. Pd_9 is a C_{2v} icosahedral fragment, again as previously reported.[14] Pd_8Ir_1 retains this structure, with the iridium dopant occupying the central site. Pd_7Ir_2 and Pd_6Ir_3 both consist of two face-sharing octahedra, with Pd_6Ir_3 having a central Ir_3 triangle and D_{3h} symmetry.

The Ir_{10} GM is a cube with a two-atom bridge over a face, forming a house-like structure, differing from the two-atom bridged edge structure reported by Wang et al., shown in Figure 4.[12] When minimized with PWscf, the BCGA-GM is found to be more favorable by 0.34 eV. This "house" structure remains the GM for $PdIr_9$, Pd_2Ir_8, Pd_3Ir_7, and Pd_4Ir_6. Pd is found to occupy preferentially the face-bridging sites, forming a Pd–Pd bond for Pd_2Ir_8. The third and fourth Pd atoms form a bond on the opposite face.

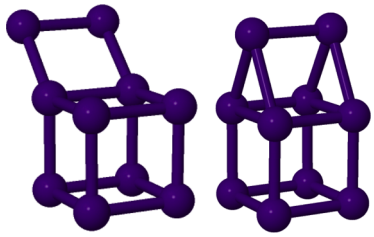

Figure 4. Lowest-energy structure reported by Wang et al. (left) and the lower-energy GM from the BCGA-DFT (right) for Ir_{10}.

The GMs for Pd_{10} and Pd_9Ir are found to be C_{3v} structures, corresponding to an incomplete centered icosahedron. For Pd_9Ir, the Ir atom occupies the exposed icosahedral core site. This differs from the edge-sharing octahedra previously reported for Pd_{10} by Ahlrichs et al., shown in Figure 5.[14] When minimized with PWscf, the BCGA-GM is found to be more favorable by 0.2 eV. The D_{2h} edge-sharing structure is, however, found as the GM for Pd_8Ir_2.

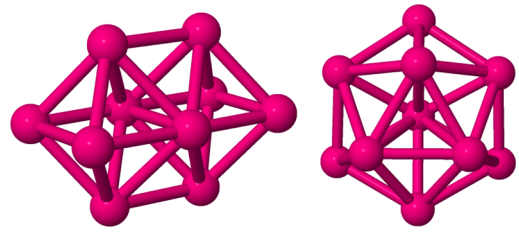

Figure 5. Lowest-energy structure reported by Ahlrichs et al. (left) and the lower-energy GM from the BCGA-DFT (right) for Pd_{10}.

The binding energies of the pure and heterometallic dimers are listed in Table 1. The triplet and quintet states for Pd_2 and Ir_2 agree with previous work.[12,14] The binding energy of Pd_2 is slightly higher than that published by Ahlrichs et al. of 0.663 eV.[14] The value of 2.28 eV for Ir_2 sits between the values of 1.58 and 2.53 eV from Wang et al. and Dixon et al., respectively.[12,13] The $5d^76s^2$ quartet state of the iridium atom is found to be 0.58 eV more favorable than the $5d^86s^1$ quartet state. The lowest spin state of PdIr (quartet) is also an intermediate between those of Ir_2 and Pd_2.

Table 1. Binding Energies (E_b) and Multiplicities ($2S + 1$) of Pd, PdIr, and Ir Dimers

dimer	E_b/eV	$(2S + 1)$
Pd_2	0.78	3
PdIr	1.41	4
Ir_2	2.28	5

The relative strengths of homo- and heteronuclear bonding can be used to predict the extent of mixing in a system. The binding energy of the heteronuclear dimer PdIr (1.41 eV) is lower than the average (1.53 eV) of the homonuclear dimers. Any structure can therefore be predicted to maximize homonuclear bonding, as seen throughout the strongly segregated structures.

The Pd–Ir phase diagram shows a significant miscibility gap below 1500 °C.[25] The bulk phase behavior of the Pd–Ir alloy system and the high Ir–Ir cohesive energy, shown in Table 2, can also be used to explain the strong demixing tendency of the clusters.

Clusters of this size have almost all atoms on the surface. The surface energies of the metals, shown in Table 2, can be used to

Table 2. Surface and Cohesive Energies for Pd and Ir[26,27]

	surface energy/J m^{-2}	cohesive energy/eV/atom
Pd	1.743	3.89
Ir	2.655	6.94

dx.doi.org/10.1021/jp408519z | J. Phys. Chem. A 2014, 118, 208–214

predict that Pd, which has the lowest surface energy, will preferentially occupy the lowest coordination sites.

Excess energies can be used to evaluate the effect of mixing in a system. The excess energy (Δ) of a system is defined in eq 1. Δ plots for N = 8−10 are shown in Figures 6−8.

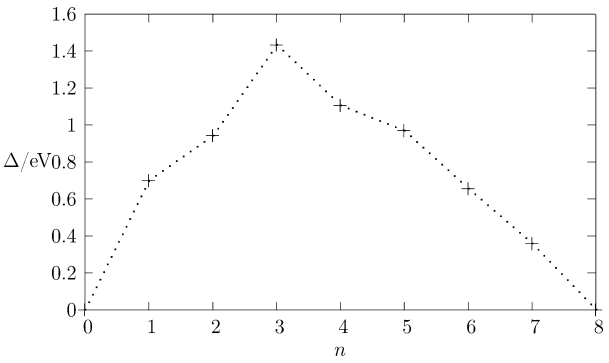

Figure 6. Plot of Δ against the number of Pd atoms for $Pd_nIr_{(8-n)}$.

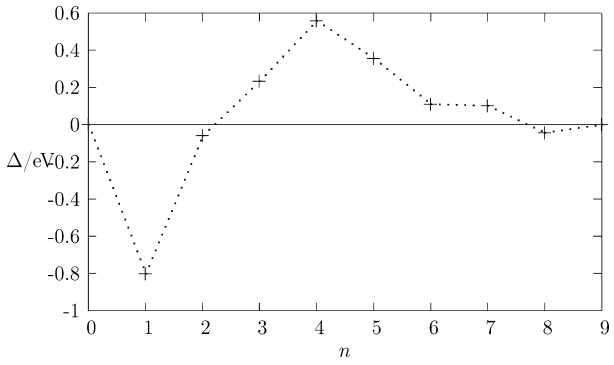

Figure 7. Plot of Δ against the number of Pd atoms for $Pd_nIr_{(9-n)}$.

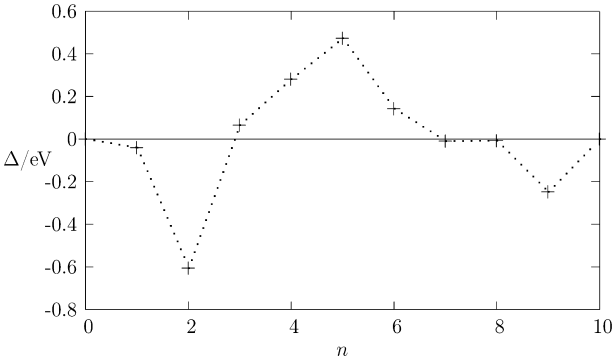

Figure 8. Plot of Δ against the number of Pd atoms for $Pd_nIr_{(10-n)}$.

The positive Δ values for $Pd_nIr_{(8-n)}$ in Figure 6 demonstrate the strong demixing tendency. The maximum Δ value is seen for Pd_3Ir_5. For the global minima of N = 9 and 10, some negative Δ values can be seen, indicating favorable mixing. Negative Δ values are seen for $PdIr_8$ and Pd_2Ir_8.

Homotops are isomers obtained by swapping the positions of different atom types.[2] The number of homotops for a system rises combinatorially with size and is maximized for 50/50 compositions. For the 10-atom house-like structures, Pd_2Ir_8, Pd_3Ir_7, and Pd_4Ir_6 have 45, 120, and 210 homotops, respectively. The number of homotops is reduced if only symmetry-inequivalent structures are considered; therefore, the numbers of homotops for Pd_2Ir_8, Pd_3Ir_7, and Pd_4Ir_6 are reduced to 15, 28, and 59, respectively. To evaluate the ability of the BCGA-DFT to find the GM, all symmetry-inequivalent cubic homotops were reminimized using PWscf for all three cluster sizes.

The homotop search confirms that the BCGA-DFT search found the lowest-energy homotop as the global minima for all but Pd_4Ir_6. This is shown for Pd_2Ir_6, Pd_1Ir_8, Pd_2Ir_7, and Pd_2Ir_8 in Figures 9−12. Figure 13 shows that the structural difference

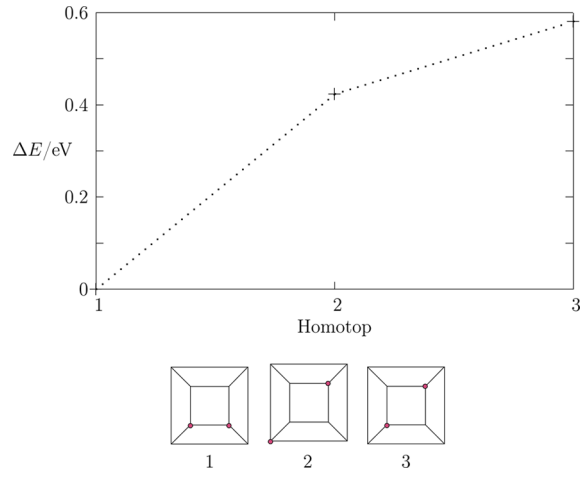

Figure 9. Relative energies of symmetry-inequivalent homotop structures for cubic Pd_2Ir_6, with homotop Schlegel diagrams displayed below in order of increasing energy. Pd is shown by circles.

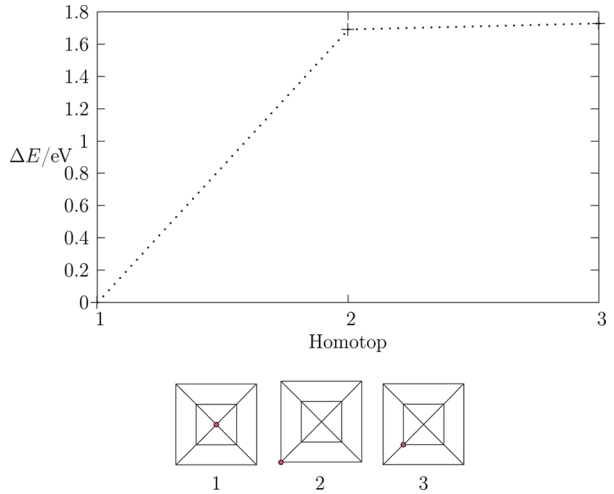

Figure 10. Relative energies of symmetry-inequivalent homotop structures for capped cubic Pd_1Ir_8.

between the two lowest-energy homotops of Pd_4Ir_6, 1 and 2, is the placement of the lower Pd−Pd bond. There are three competing factors that determine the homotop stability. First, Pd atoms preferentially tend to occupy low-connectivity sites (due to the relative weakness of Pd−M bonds and lower surface energy). Second, Pd typically occupies capping sites, thereby minimizing distortion of the Ir_8 cube. Finally, Pd atoms tend to segregate together as this maximizes the number of (stronger) Ir−Ir bonds.

During the QE geometry optimization, homotop 32 for Pd_4Ir_6 underwent a barrierless transition to the overall GM structure (homotop 2). Figure 14 shows the structural

dx.doi.org/10.1021/jp408519z | J. Phys. Chem. A 2014, 118, 208−214

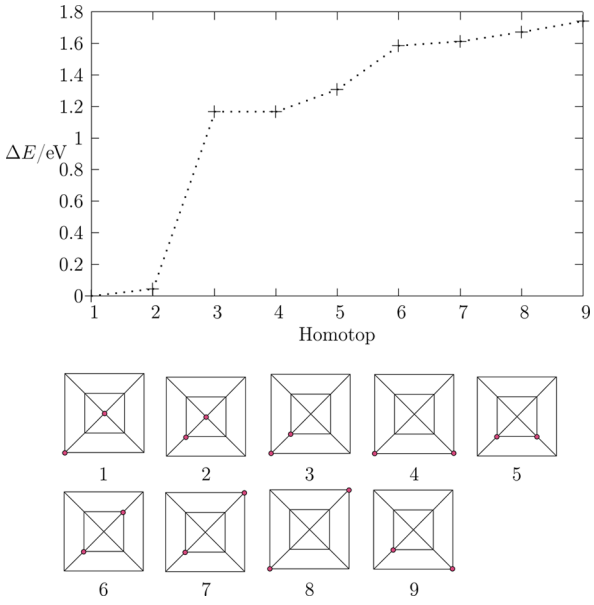

Figure 11. Relative energies of symmetry-inequivalent homotop structures for capped cubic Pd_2Ir_7.

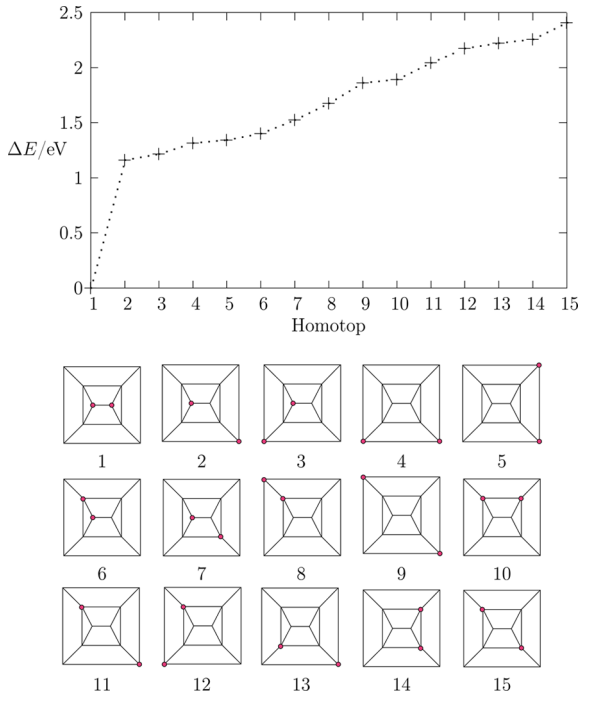

Figure 12. Relative energies of symmetry-inequivalent homotop structures for house-like Pd_2Ir_8.

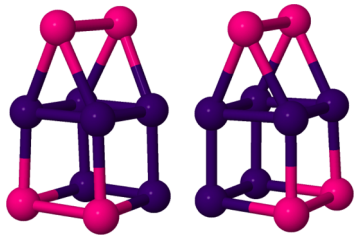

Figure 13. Homotop structures of Pd_4Ir_6: homotop 1 (left) and homotop 2 (right).

reorganization through a structure composed of three face-sharing trigonal prisms, taken from the L-BFGS minimization pathway.

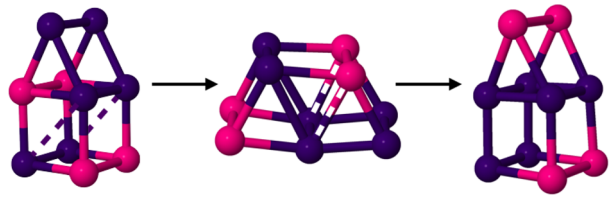

Figure 14. Structural rearrangement of Pd_4Ir_6 homotop 32 to 2 via the face-sharing trigonal prism structure; bond formation and breaking are shown by dashed lines and striped line bonds, respectively.

Tables 3–5 display the effect of restricting spin in NWChem reoptimizations of the BCGA-DFT minima for $Pd_nIr_{(N-n)}$ N =

Table 3. Relative Energies (ΔE/eV) for Various Multiplicities ($2S + 1$) of $Pd_nIr_{(8-n)}$ Clusters

Ir_8		$PdIr_7$		Pd_2Ir_6	
$(2S + 1)$	ΔE	$(2S + 1)$	ΔE	$(2S + 1)$	ΔE
1	0	2	0	1	0.563
3	0.102	4	0.179	3	0.137
5	0.108	6	0.162	5	0.127
7	0.225	8	0.108	7	0.141
9	0.245	10	0.122	9	0.08
11	0.252			11	0
13	0.104			13	0.274
15	1.661			15	0.916
Pd_3Ir_5		Pd_4Ir_4		Pd_5Ir_3	
$(2S + 1)$	ΔE	$(2S + 1)$	ΔE	$(2S + 1)$	ΔE
2	0.404	1	0.629	2	0
4	0.429	3	0.272	4	0.173
6	0.284	5	0.189	6	0.32
8	0.075	7	0.125	8	0.408
10	0	9	0.027	10	0.392
12	0.117	11	0		
14	0.392	13	0.122		
16	2.078	15	1.866		
Pd_6Ir_2		Pd_7Ir		Pd_8	
$(2S + 1)$	ΔE	$(2S + 1)$	ΔE	$(2S + 1)$	ΔE
1	0.49	2	0.214	1	0.13
3	0.171	4	0.095	3	0.021
5	0.005	6	0	5	0
7	0	8	0.147	7	0.568
9	0.394	10	0.579	9	1.085

8–10. Each structure was reoptimized for its first five lowest multiplicities, the most favorable spin-state being the lowest-energy multiplicity. For those structures whose lowest-energy multiplicity was the highest of these values, three extra spin states were considered; this was the case for Pd_2Ir_6, Pd_3Ir_5, and Pd_4Ir_4. Previous work on Ir_8 has shown it to favor a 13-et state.[13] Our results suggest that Ir_8 has a singlet state, with a low-lying (ΔE = 0.1 eV) triplet and 13-et state. Ir_9 and Ir_{10} are found to have sextet and triplet ground states, respectively.

The lowest-energy multiplicities of Pd_8, Pd_9, and Pd_{10} are a quintet, quintet, and septet, respectively. Pd_8 is found to favor a higher spin state than the triplet previously reported.[14] There is

dx.doi.org/10.1021/jp408519z | J. Phys. Chem. A 2014, 118, 208–214

Table 4. Relative Energies (ΔE/eV) for Various Multiplicities ($2S + 1$) of $Pd_nIr_{(9-n)}$ Clusters

Ir_9		$PdIr_8$		Pd_2Ir_7	
$(2S + 1)$	ΔE	$(2S + 1)$	ΔE	$(2S + 1)$	ΔE
2	0.028	1	0	2	0
4	0.008	3	0.128	4	0.089
6	0	5	0.192	6	0.15
8	0.124	7	0.354	8	0.157
10	0.214	9	0.488	10	0.173
Pd_3Ir_6		Pd_4Ir_5		Pd_5Ir_4	
$(2S + 1)$	ΔE	$(2S + 1)$	ΔE	$(2S + 1)$	ΔE
1	0.255	2	0.439	1	0.351
3	0	4	0.301	3	0.153
5	0.042	6	0.229	5	0
7	0.175	8	0.113	7	0.022
9	0.049	10	0	9	0.033
		12	0.054		
		14	0.29		
		16	1.707		
Pd_6Ir_3		Pd_7Ir_2		Pd_8Ir	
$(2S + 1)$	ΔE	$(2S + 1)$	ΔE	$(2S + 1)$	ΔE
2	0	1	0.163	2	0.35
4	0.107	3	0	4	0.192
6	0.277	5	0.12	6	0.078
8	0.453	7	0.244	8	0
10	0.66	9	0.244	10	0.497
Pd_9					
$(2S + 1)$	ΔE				
1	0.271				
3	0.098				
5	0				
7	0.086				
9	0.788				

Table 5. Relative Energies (ΔE/eV) for Various Multiplicities ($2S + 1$) of $Pd_nIr_{(10-n)}$ Clusters

Ir_{10}		$PdIr_9$		Pd_2Ir_8	
$(2S + 1)$	ΔE	$(2S + 1)$	ΔE	$(2S + 1)$	ΔE
1	0.168	2	0.14	1	0
3	0	4	0	3	0.7
5	0.184	6	0.173	5	0.159
7	0.244	8	0.375	7	0.4
9	0.389	10	0.492	9	0.651
Pd_3Ir_7		Pd_4Ir_6		Pd_5Ir_5	
$(2S + 1)$	ΔE	$(2S + 1)$	ΔE	$(2S + 1)$	ΔE
2	0	1	0.254	2	0.095
4	0.005	3	0	4	0.275
6	0.164	5	0.112	6	0
9	0.264	7	0.203	8	0.047
10	0.434	9	0.371	10	0.017
Pd_6Ir_4		Pd_7Ir_3		Pd_8Ir_2	
$(2S + 1)$	ΔE	$(2S + 1)$	ΔE	$(2S + 1)$	ΔE
1	0.273	2	0	1	0.373
3	0.046	4	0.132	3	0.112
5	0	6	0.243	5	0.004
7	0.08	8	0.291	7	0
9	0.098	10	0.44	9	0.067
Pd_9Ir		Pd_{10}			
$(2S + 1)$	ΔE	$(2S + 1)$	ΔE		
2	0.4	1	0.568		
4	0.0262	3	0.263		
6	0.183	5	0.176		
8	0	7	0		
10	0.356	9	0.433		

no clear pattern of lowest-energy spin states as a function of composition for the mixed Pd−Ir clusters.

The role of spin was further investigated through spin-restricted reoptimizations of three lowest metastable minima, for Ir_8, $PdIr_7$, and Pd_2Ir_6. For each composition, the GM structure did not change (see the Supporting Information).

CONCLUSIONS

The use of the BCGA-DFT method has allowed the global optimization of $Pd_nIr_{(N-n)}$ $N = 8-10$ nanoalloys. The ability to explore the potential energy surface of the system at the DFT level has yielded the identification of families of cubic structures for pure Ir and Ir-rich PdIr nanoalloys, which are typically not found as low-energy isomers using empirical potentials. Results for the monometallic species were found to be largely in agreement with those previously reported.[12−14] The ability of the searches to find the putative GM was evaluated by assessing the relative energies of symmetry-inequivalent homotops of cubic minima. The BCGA-DFT searches were found to be very reliable.

Through the use of spin-restricted reoptimizations on BCGA global minima, the role of spin in the system has been considered. Spin has been shown to vary widely depending on composition, showing no real trend in lowest-energy multiplicities. The spins of the monometallic species are found to be in good agreement with those from previous studies.[13,14] Further spin-restricted reoptimizations of metastable minima have no change in the GM structure; however, any future studies of this system must include consideration of spin.

Previous work on pure Ir clusters has indicated a simple cubic to bulk FCC transition at 48 atoms.[12] In future work, the cubic structures of pure Ir and Ir-rich nanoalloys will be explored further. These structural studies will be important in future computational studies of catalysis on Pd−Ir nanoalloys.

ASSOCIATED CONTENT

Supporting Information

Binding energies, structures, and point group symmetries for all $Pd_nIr_{(N-n)}$ ($m = 8-10$) clusters, relative energies and homotop Schlegel diagrams for Pd_3Ir_7 and Pd_4Ir_6, and results of spin-restricted reoptimizations of the BCGA-DFT global minima and the three lowest metastable minima for Ir_8, $PdIr_7$, and Pd_2Ir_6. This material is available free of charge via the Internet at http://pubs.acs.org.

AUTHOR INFORMATION

Corresponding Author

*E-mail: r.l.johnston@bham.ac.uk.

Notes

The authors declare no competing financial interest.

ACKNOWLEDGMENTS

J.B.A.D. thanks the School of Chemistry, University of Birmingham, and EPSRC for his Ph.D. scholarship and Paul C. Jennings for helpful discussions. The authors acknowledge

the Engineering and Physical Sciences Research Council, U.K. (EPSRC) for funding under Critical Mass Grant EP/J010804/1 "TOUCAN: Towards an Understanding of Catalysis on Nanoalloys". Calculations were performed via our membership of the U.K.'s HPC Materials Chemistry Consortium, which is funded by EPSRC (EP/F067496); this work made use of the facilities of HECToR, the U.K.'s national high-performance computing service, which is provided by UoE HPCx Ltd. at the University of Edinburgh, Cray Inc., and NAG Ltd. and funded by the Office of Science and Technology through EPSRC's High End Computing Programme. Calculations were also performed on the EPSRC-funded MidPlus HPC facility, Grant EP/K000128/1.

REFERENCES

(1) Sinfelt, J. H. *Bimetallic Catalysts: Discoveries, Concepts, and Applications*; Wiley: New York, 1983.
(2) Ferrando, R.; Jellinek, J.; Johnston, R. L. Nanoalloys: From Theory to Applications of Alloy Clusters and Nanoparticles. *Chem. Rev.* **2008**, *108*, 845−910.
(3) Johnston, R. L.; Wilcoxon, J. P. *Metal Nanoparticles and Nanoalloys*, 1st ed.; Elsevier Ltd.: New York, 2012; Vol. 3, pp 1−42.
(4) Wales, D. J. Global Optimization by Basin-Hopping and the Lowest Energy Structures of Lennard-Jones Clusters Containing up to 110 Atoms. *J .Chem. Phys.* **1997**, *101*, 5111−5116.
(5) Johnston, R. L. Evolving Better Nanoparticles: Genetic Algorithms for Optimising Cluster Geometries. *Dalton Trans.* **2003**, 4193−4207.
(6) Uzun, A.; Dixon, D. A.; Gates, B. C. Prototype Supported Metal Cluster Catalysts: Ir_4 and Ir_6. *ChemCatChem* **2011**, *3*, 95−107.
(7) Rocha, A.; Moreno, E.; da Silva, G.; Zotin, J.; Faro, A. Tetralin Hydrogenation on Dealuminated Y Zeolite-Supported Bimetallic Pd−Ir Catalysts. *Catal. Today* **2008**, *133*−*135*, 394−399.
(8) Piccolo, L.; Nassreddine, S.; Aouine, M.; Ulhaq, C.; Geantet, C. Supported Ir−Pd Nanoalloys: Size-Composition Correlation and Consequences on Tetralin Hydroconversion Properties. *J. Catal.* **2012**, *292*, 173−180.
(9) López-De Jesús, Y. M.; Johnson, C. E.; Monnier, J. R.; Williams, C. T. Selective Hydrogenation of Benzonitrile by Alumina-Supported Ir−Pd Catalysts. *Top. Catal.* **2010**, *53*, 1132−1137.
(10) Morfin, F.; Nassreddine, S.; Rousset, J. L.; Piccolo, L. Nanoalloying Effect in the Preferential Oxidation of CO over Ir−Pd Catalysts. *ACS Catal.* **2012**, *2*, 2161−2168.
(11) Zhang, W.; Xiao, L.; Hirata, Y.; Pawluk, T.; Wang, L. The Simple Cubic Structure of Ir Clusters and the Element Effect on Cluster Structures. *Chem. Phys. Lett.* **2004**, *383*, 67−71.
(12) Pawluk, T.; Hirata, Y.; Wang, L. Studies of Iridium Nanoparticles Using Density Functional Theory Calculations. *J. Phys. Chem. B* **2005**, *109*, 20817−20823.
(13) Chen, M.; Dixon, D. A. Low-Lying Electronic States of Irn Clusters with n = 2−8 Predicted at the DFT, CASSCF and CCSD(T) Levels. *J. Phys. Chem. A* **2013**, *117*, 3676−3688.
(14) Nava, P.; Sierka, M.; Ahlrichs, R. Density Functional Study of Palladium Clusters. *Phys. Chem. Chem. Phys.* **2003**, *5*, 3372−3381.
(15) Giannozzi, P.; Baroni, S. QUANTUM ESPRESSO: A Modular and Open-Source Software Project for Quantum Simulations of Materials. *J. Phys.: Condens. Matter* **2009**, *21*, 395502.
(16) Heiles, S.; Logsdail, A. J.; Schäfer, R.; Johnston, R. L. Dopant-Induced 2D−3D Transition in Small Au-Containing Clusters: DFT-Global Optimisation of 8-Atom Au−Ag Nanoalloys. *Nanoscale* **2012**, *4*, 1109−1115.
(17) Heiles, S.; Johnston, R. L. Global Optimization of Clusters using Electronic Structure Methods. *Int. J. Quantum Chem.* **2013**, *113*, 2091−2109.
(18) Sansonetti, J. E.; Martin, W. C. Handbook of Basic Atomic Spectroscopic Data. *J. Phys. Chem. Ref. Data* **2005**, *34*, 1777−1781.
(19) Valiev, M.; Bylaska, E.; Govind, N.; Kowalski, K.; Straatsma, T.; Van Dam, H.; Wang, D.; Nieplocha, J.; Apra, E.; Windus, T.; de Jong, W. NWChem: A Comprehensive and Scalable Open-Source Solution for Large Scale Molecular Simulations. *Comput. Phys. Commun.* **2010**, *181*, 1477−1489.
(20) Deaven, D.; Ho, K. Molecular Geometry Optimization with a Genetic Algorithm. *Phys. Rev. Lett.* **1995**, *75*, 288−291.
(21) Blöchl, P. Projector Augmented-Wave Method. *Phys. Rev. B* **1994**, *50*, 17953.
(22) Perdew, J.; Burke, K.; Wang, Y. Generalized Gradient Approximation for the Exchange−Correlation Hole of a Many-Electron System. *Phys. Rev. B* **1996**, *54*, 533−539.
(23) Ernzerhof, M.; Scuseria, G. E. Assessment of the Perdew−Burke−Ernzerhof Exchange−Correlation Functional. *J. Chem. Phys.* **1999**, *110*, 5029.
(24) Weigend, F.; Ahlrichs, R. Balanced Basis Sets of Split Valence, Triple Zeta Valence and Quadruple Zeta Valence Quality for H to Rn: Design and Assessment of Accuracy. *Phys. Chem. Chem. Phys.* **2005**, *7*, 3297−305.
(25) Tripathi, S. N.; Bharadwaj, S. R.; Chandrasekharaiah, M. S. The Ir−Pd (Iridium−Palladium) System. *J. Phase Equilib.* **1991**, *12*, 603−605.
(26) Tyson, W.; Miller, W. Surface Free Energies of Solid Metals: Estimation from Liquid Surface Tension Measurements. *Surf. Sci.* **1977**, *62*, 267−276.
(27) Kittel, C. *Introduction to Solid State Physics*, 6th ed.; John Wiley & Sons: New York, 1986; p 55.